IET Generation, Transmission & Distribution

WILEY

The Institution of Engineering and Technology

ORIGINAL RESEARCH OPEN ACCESS

Investigating Disturbance-Induced Misoperation of Grid-Following Inverter-Based Resources

Negar Karimipour[1] | Mohammadreza F. M. Arani[1] | Amir Abiri Jahromi[2]

[1]Department of Electrical, Computer, and Biomedical Engineering, Toronto Metropolitan University, Toronto, Canada | [2]School of Electronic and Electrical Engineering, University of Leeds, Leeds, UK

Correspondence: Mohammadreza F. M. Arani (marani@torontomu.ca)

Received: 26 October 2024 | **Revised:** 25 February 2025 | **Accepted:** 6 March 2025

Funding: Financial support was provided by the NSERC Discovery Grants Program.

ABSTRACT

The rapid integration of grid-following inverter-based resources (GFL-IBRs) has increased the importance of their dynamic behaviour during disturbances. Simultaneously, there are increasing number of reports about the misoperation or inadvertent disconnection of GFL-IBRs during disturbances. This paper attempts to shed light on one of the potential root causes of disturbance-induced misoperations of GFL-IBRs. A framework is presented to quantify voltage drop and voltage phase angle jump that appear at the terminals of GFL-IBRs immediately after the inception of various events in the grid such as faults, and tripping of generators and transmission lines. We demonstrate voltage drop and voltage phase angle jump in the upstream grid due to various disturbances may transform into severe voltage drop and voltage phase angle jump at the terminals of GFL-IBRs. The combination of voltage drop and voltage phase angle jump that appear at the terminals of GFL-IBRs is identified as one of the root causes of their misoperation. Therefore, system-wide studies are required to evaluate the dynamic performance of GFL-IBRs rather than sole compliance with standards. The importance of system-wide studies is demonstrated through IEEE 39-bus test system. The impact of voltage drop and voltage phase angle jump in the upstream grid on the dynamic performance of GFL-IBRs is demonstrated using electromagnetic transient studies.

1 | Introduction

Electric power systems are on the cusp of a major transformation moving away from synchronous generators towards inverter-based resources (IBRs) to achieve zero-carbon systems [1, 2]. This paradigm shift demands revisiting the performance of IBRs during disturbances. The IBRs traditionally were expected to stay connected to the grid only during normal operating conditions and to disconnect from the grid during disturbances. Yet, this practice is not acceptable anymore in power systems with the increasing penetration levels of IBRs as it may cause large disturbances similar to the Blue Cut Fire event in Southern California in 2016 [3].

To address this challenge, standards such as IEEE 2800 and IEEE 1547 establish the minimum performance requirements of IBRs during disturbances [4, 5]. Nevertheless, these standards cannot enforce uniformity and consistency between the responses of IBRs during disturbances because there is no standardisation for the implementation of the control of IBRs [6]. This has already resulted in the misoperation or inadvertent disconnection of grid-following inverter-based resources (GFL-IBRs) during disturbances as evidenced by the events in Odessa, Texas in 2021 and 2022 [7, 8].

The focus of most studies in the literature has been on investigating the compliance of the response of IBRs to standards or developing generic models of GFL-IBRs for dynamic studies rather than examining the root cause of disturbance-induced misoperation of GFL-IBRs. A test plan is presented in [9] to verify that each grid support function of distributed energy resources operates in accordance with standards. A test plan is presented in [10] to examine the grid support functions of solar photovoltaic (PV) inverters in Hawaiian electric distribution feeders. A set of tests are presented in [11] to examine the impact of grid support functions in inverters on anti-islanding detection. The grid support capability and performance of four inverters have been examined in [12] for Florida Power and Light Company. The compliance of converter-interfaced resources during balanced and unbalanced faults with grid code has been studied in [13] and [14]. A voltage support control strategy is proposed in [15] to meet grid code requirements. A fault ride through method is proposed in [16] and its compliance with the reliability guideline of the North American Electric Reliability Corporation and other grid codes is investigated.

The generic models of PV systems developed by the Western Electric Coordinating Council (WECC) are presented in [17]. The generic PV models developed by WECC are implemented and validated in [18] using DIgSILENT PowerFactory. The generic Type 4 wind turbine models developed by the International Electrotechnical Commission (IEC) and WECC are tested and validated in [19]. Yet, disturbance-induced misoperation of GFL-IBRs has rarely been investigated in the literature [20–22]. In [20, 21], the dynamic responses of off-the-shelf residential PV inverters during disturbances are experimentally examined. It is demonstrated that disturbances in power systems can cause disconnection of the PV inverters from the grid in most cases. In [22], the large voltage phase angle jumps experienced by GFL-IBRs due to voltage drops are investigated. Moreover, the impact of frequency support and voltage support in suppressing large voltage phase angle jumps due to voltage drops are examined and discussed.

This paper begins by evaluating and comparing voltage drop and voltage phase angle jump at the terminals of synchronous generators and GFL-IBRs due to voltage drop and voltage phase angle jump in the upstream grid. It is demonstrated that in contrast to synchronous generators, GFL-IBRs can experience severe voltage drop and voltage phase angle jump at their terminals due to voltage drop and voltage phase angle jump in the upstream grid which triggers their misoperation. We also examine and discuss the influencing factors on determining voltage drop and voltage phase angle jump at the terminals of GFL-IBRs. The aforementioned analyses highlighted the need for characterising disturbance-induced voltage drop and voltage phase angle jump at the location of GFL-IBRs using system-wide studies. The main contributions of this paper are as follows:

- Disturbance-induced voltage drop and voltage phase angle jump at the terminals of synchronous generators and GFL-IBRs are compared and their differences are highlighted.
- The influencing factors on determining voltage drop and voltage phase angle jump at the terminals of GFL-IBRs are examined and discussed.

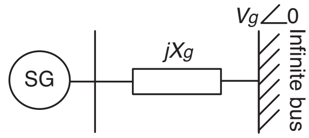

FIGURE 1 | Single machine infinite bus model.

- It is demonstrated that disturbance-induced voltage drop and voltage phase angle jump in the upstream grid can trigger the misoperation of GFL-IBRs.
- It is demonstrated that compliance with existing standards is not sufficient and system-wide studies are required to test and validate the dynamic performance of GFL-IBRs.

The remainder of the paper is organized as follows. The classic single machine infinite bus model is employed in Section 2 to analytically quantify and compare voltage drop and voltage phase angle jump at the terminals of synchronous generators and GFL-IBRs immediately after the inception of disturbances. Moreover, the influencing factors on determining voltage drop and voltage phase angle jump at the terminals of GFL-IBRs are discussed. In Section 3, system-wide analyses are employed to characterise voltage drop and voltage phase angle jump in the upstream bus of a GFL-IBR. The impact of voltage drop and voltage phase angle jump in the upstream grid on the dynamic performance of GFL-IBRs is demonstrated in Section 4 using electromagnetic transient (EMT) studies before concluding the paper in Section 5.

2 | An Elementary View of Disturbance-Induced Voltage Characteristics at the Terminal of SGs and GFL-IBRs

In this section, we compare the characteristics of voltage drops and voltage phase angle jumps that appear at the terminals of synchronous generators and GFL-IBRs due to various disturbances in the upstream grid. The classic single machine infinite bus model is employed to derive the characteristics of voltage drops and voltage phase angle jumps.

2.1 | Synchronous Generators

The classic single machine infinite bus model for a synchronous generator is demonstrated in Figure 1. Without loss of generality, the pre-disturbance voltage phase angle of the infinite bus is considered as a reference, that is, $\angle V_g = 0$. The disturbance in the upstream grid is modelled by voltage drop equal to $1 - \alpha$ per unit and voltage phase angle jump equal to θ at the infinite bus. Thus, voltage at the infinite bus is $\alpha V_g \angle\theta$ at the instant of the disturbance inception. The pre-disturbance voltage phasor at the terminal of the synchronous generator is given in (1). The voltage phasor at the instant of the disturbance inception is given in (2).

$$\overline{V}_t^{\text{pre}} = \frac{X_s}{X_s + X_g} V_g \angle 0 + \frac{X_g}{X_s + X_g} E_f \angle\delta \tag{1}$$

$$\overline{V}_t^{\text{instant}} = \frac{X_s}{X_s + X_g} \alpha V_g \angle\theta + \frac{X_g}{X_s + X_g} E_f \angle\delta \tag{2}$$

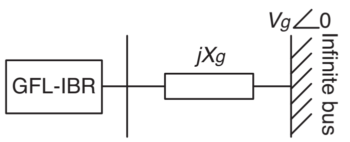

FIGURE 2 | Single inverter infinite bus model.

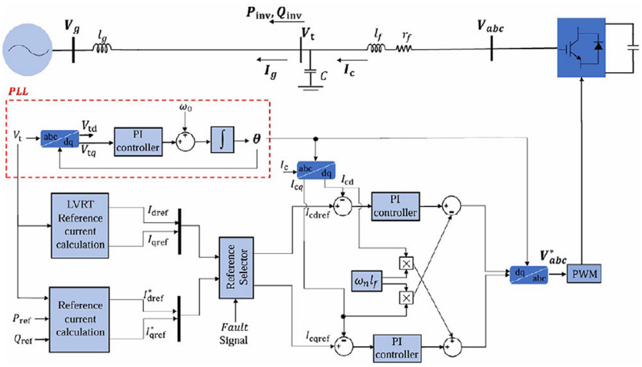

FIGURE 3 | The control block diagram of GFL-IBRs [23].

where X_s and X_g denote the reactance of the synchronous generator and the reactance of the transmission line, respectively. E_f and δ denote the field voltage and the rotor angle of the synchronous generator.

The pre-disturbance voltage magnitude and voltage phase angle at the terminal of the synchronous generator are given in (3) and (5), respectively. Voltage magnitude and voltage phase angle at the instant of the disturbance inception are given in (4) and (6), respectively.

$$|\bar{V}_t^{\text{pre}}| = \sqrt{\left(\frac{X_s}{X_s+X_g}V_g + \frac{X_g}{X_s+X_g}E_f\cos\delta\right)^2 + \left(\frac{X_g}{X_s+X_g}E_f\sin\delta\right)^2} \tag{3}$$

$$|\bar{V}_t^{\text{instant}}| = \sqrt{\left(\frac{\alpha X_s}{X_s+X_g}V_g\cos\theta + \frac{X_g}{X_s+X_g}E_f\cos\delta\right)^2 + \left(\frac{\alpha X_s}{X_s+X_g}V_g\sin\theta + \frac{X_g}{X_s+X_g}E_f\sin\delta\right)^2} \tag{4}$$

$$\angle\overline{V}_t^{\text{pre}} = \arctan\frac{X_gE_f\sin\delta}{X_sV_g + X_gE_f\cos\delta} \tag{5}$$

$$\angle\overline{V}_t^{\text{instant}} = \arctan\frac{\alpha X_sV_g\sin\theta + X_gE_f\sin\delta}{\alpha X_sV_g\cos\theta + X_gE_f\cos\delta} \tag{6}$$

2.2 | Grid-Following Inverter-Based Resources

The single machine infinite bus model for a GFL-IBR is demonstrated in Figure 2. The control block diagram of the conventional GFL-IBRs used in this paper is provided in Figure 3. The parameters of the controller are provided in the Appendix. Again, we consider the pre-disturbance voltage phase angle of the infinite bus as a reference, that is, $\angle V_g = 0$. The disturbance in the upstream grid is modelled by voltage drop equal to $1-\alpha$ per unit and voltage phase angle jump equal to θ at the infinite bus.

Thus, voltage at the infinite bus is $\alpha V_g\angle\theta$ at the instant of the disturbance inception. The pre-disturbance voltage phasor at the terminal of the GFL-IBR is given in (7). Voltage phasor at the instant of the disturbance inception is given in (8).

$$\overline{V}_t^{\text{pre}} = V_g\angle 0 + jX_gI_c\angle\theta_c \tag{7}$$

$$\overline{V}_t^{\text{instant}} = \alpha V_g\angle\theta + jX_gI_c\angle\theta_c \tag{8}$$

where X_g denotes the reactance of the transmission line. The GFL-IBR is modelled by a current source with the current $I_c\angle\theta_c$. It is worth noting that the current of the GFL-IBR in (8) is considered to be equal to the current in (7). This is because (8) is derived at the instant immediately after the inception of the disturbance. Therefore, the fault ride-through mechanism of the GFL-IBR is not activated yet.

The pre-disturbance voltage magnitude and voltage phase angle at the terminal of the GFL-IBR are given in (9) and (11), respectively. Voltage magnitude and voltage phase angle at the instant of the disturbance inception are given in (10) and (12), respectively.

$$|\overline{V}_t^{\text{pre}}| = \sqrt{(V_g - X_gI_c\sin\theta_c)^2 + (X_gI_c\cos\theta_c)^2} \tag{9}$$

$$|\bar{V}_t^{\text{instant}}| = \sqrt{(\alpha V_g\cos\theta - X_gI_c\sin\theta_c)^2 + (\alpha V_g\sin\theta + X_gI_c\cos\theta_c)^2} \tag{10}$$

$$\angle\overline{V}_t^{\text{pre}} = \arctan\frac{X_gI_c\cos\theta_c}{V_g - X_gI_c\sin\theta_c} \tag{11}$$

$$\angle\overline{V}_t^{\text{instant}} = \arctan\frac{\alpha V_g\sin\theta + X_gI_c\cos\theta_c}{\alpha V_g\cos\theta - X_gI_c\sin\theta_c} \tag{12}$$

2.3 | Comparative Study of Voltage Characteristics at the Terminal of SGs and GFL-IBRs at the Instant of Disturbance Inception

In this section, the formulations derived in Sections 2.1 and 2.2 are used to compare voltage characteristics at the terminal of synchronous generators and GFL-IBRs at the instant of disturbance inception. In order to develop insight and avoid complexity, voltage drops and voltage phase angle jumps that appear at the terminals of synchronous generators and GFL-IBRs are demonstrated for the following three cases.

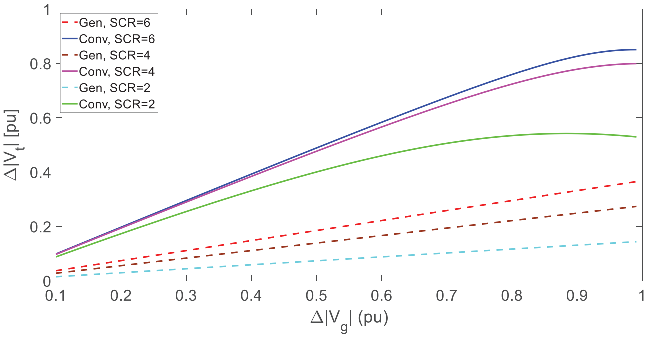

FIGURE 4 | Change in the voltage magnitude due to voltage drop at the infinite bus for different grid strengths. Synchronous generator and GFL-IBR cases are shown by dashed and solid curves, respectively.

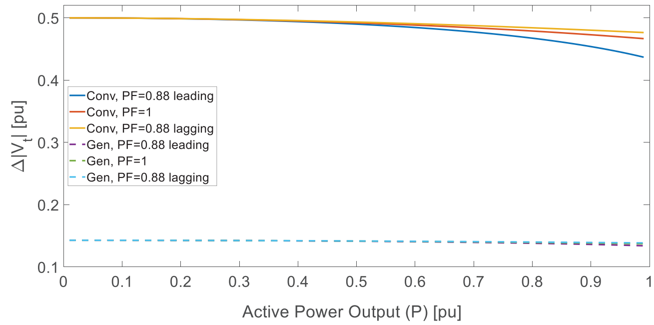

FIGURE 5 | Change in the voltage magnitude due to voltage drop equal to 0.5 pu at the infinite bus for different operating points. Synchronous generator and GFL-IBR cases are shown by dashed and solid curves, respectively.

2.3.1 | Voltage Drop at the Infinite Bus in the Absence of Voltage Phase Angle Jump

Voltage characteristics at the terminal of synchronous generators and GFL-IBRs are demonstrated in Figure 4 when voltage drop occurs at the infinite bus without voltage phase angle jump.

As illustrated in Figure 4, voltage drop at the terminal of the synchronous generator depends on voltage drop at the infinite bus. Nevertheless, voltage drop at the terminal of the synchronous generator is comparatively much smaller than voltage drop at the infinite bus. This behaviour is due to the voltage source nature of synchronous generators. It is further worth noting that short circuit ratio of the grid has intangible impact on voltage drop at the terminal of the synchronous generator.

In contrast to synchronous generators, voltage drop at the infinite bus creates significant voltage drop at the terminal of GFL-IBRs as illustrated in Figure 4. This behaviour is due to the current source nature of GFL-IBRs. It can further be observed in Figure 4 that the SCR of the grid is a crucial factor in determining the relationship between voltage drop at the infinite bus and voltage drop at the terminal of GFL-IBRs.

Another influencing factor that impacts the relationship between voltage drop at the infinite bus and voltage drop at the terminal of GFL-IBRs is the operating point of the GFL-IBR as illustrated in Figure 5. As illustrated in Figure 5, voltage drop at the terminal of a GFL-IBR increases from 0.43 to 0.5 pu when the injected active power of the GFL-IBR changes from 1 to 0 pu for voltage drop equal to 0.5 pu at the infinite bus. Figure 5 also underlines the impact of the output power factor of the GFL-IBR. In contrast to GFL-IBRs, voltage drop at the terminal of a synchronous generator is unaffected by the active and reactive output of the synchronous generator.

As illustrated in Figure 6, voltage phase angle jump at the terminal of a synchronous generator is almost independent of voltage drop at the infinite bus regardless of the grid strength. Again, this is because of the voltage source nature of synchronous generators.

In contrast to synchronous generators, voltage phase angle jump at the terminal of a GFL-IBR highly depends on voltage drop at the infinite bus. It can be observed in Figure 6 that the SCR of the

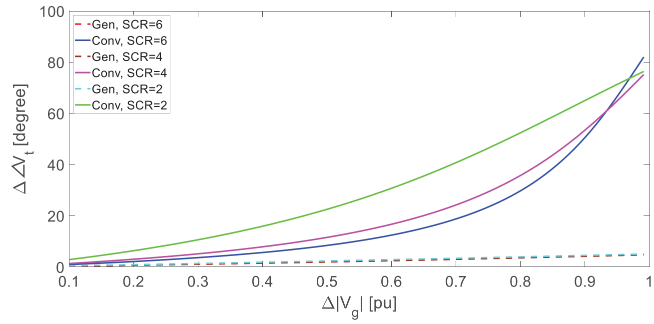

FIGURE 6 | Change in the voltage phase angle jump due to voltage drop at the infinite bus for different grid strengths. Synchronous generator and GFL-IBR cases are shown by dashed and solid curves, respectively.

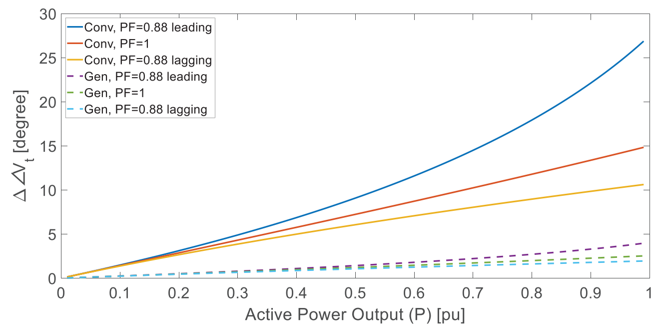

FIGURE 7 | Change in the voltage phase angle jump due to voltage drop equal to 0.5 pu at the infinite bus for different operating points. Synchronous generator and GFL-IBR cases are shown by dashed and solid curves, respectively.

grid is a critical factor in determining the relationship between voltage drop at the infinite bus and voltage phase angle jump at the terminal of GFL-IBRs. This behaviour is again due to the current source nature of GFL-IBRs.

Another determining factor that impacts the relationship between voltage drop at the infinite bus and voltage phase angle jump at the terminal of GFL-IBRs is the operating point of the IBR as illustrated in Figure 7. As illustrated in Figure 7, voltage phase angle jump at the terminal of the GFL-IBR increases from 0° to 27° when the injected active power of the GFL-IBR changes

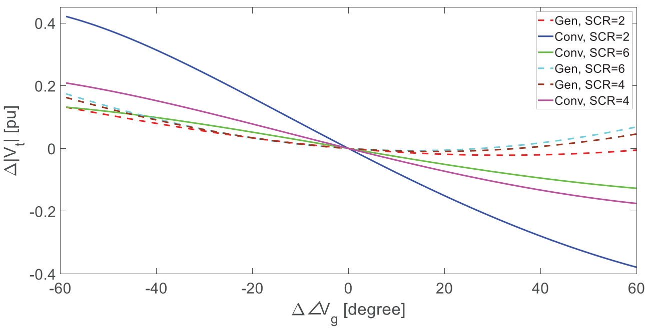

FIGURE 8 | Change in the voltage magnitude due to voltage phase angle jump at the infinite bus for different grid strengths. Synchronous generator and GFL-IBR cases are shown by dashed and solid curves, respectively.

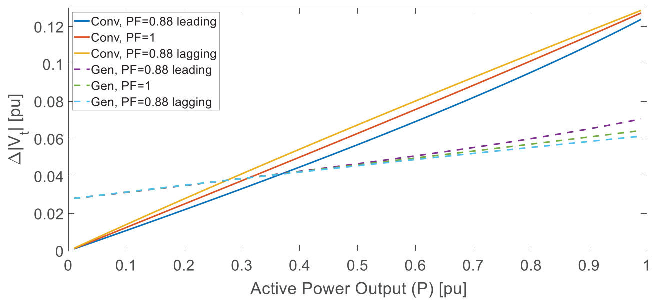

FIGURE 9 | Change in the voltage magnitude due to voltage phase angle jump equal to −30° at the infinite bus for different operating points. Synchronous generator and GFL-IBR cases are shown by dashed and solid curves, respectively.

from 0 to 1 pu for voltage drop equal to 0.5 pu at the infinite bus. Figure 7 also underlines the impact of the output power factor of the GFL-IBR. For example, voltage phase angle jump increases from 11° to 27° when power factor changes from 0.88 lagging to 0.88 leading.

As demonstrated in this section, voltage drops at the upstream grid can create severe voltage phase angle jumps at the terminal of GFL-IBRs. The protection of GFL-IBRs are required to disconnect the inverter within sub-cycle-to-cycle for voltage phase angle jumps larger than 20° based on the IEEE standard 1547. This may create challenges for the successful fault ride-through of GFL-IBRs depending on the dynamics of the phase-locked loop (PLL) of the GFL-IBRs. The impact of PLL dynamics and possible loss of synchronism due to voltage drop at the upstream grid has been investigated in [22]. Nevertheless, the impact of voltage phase angle jump at the upstream grid on voltage drop and voltage phase angle jump has never been studied previously in the literature which is discussed in the next section.

2.3.2 | Voltage Phase Angle Jump at the Infinite Bus in the Absence of Voltage Drop

Voltage characteristics at the terminal of synchronous generators and GFL-IBRs are demonstrated in Figure 8 when voltage phase angle jump occurs at the infinite bus without voltage drop.

As illustrated in Figure 8, voltage phase angle jump at the infinite bus has trivial impact on voltage drop at the terminal of a synchronous generator. As shown in Figure 8, even voltage phase angle jumps as large as 60° does not create voltage drop more than 0.2 pu at the terminal of a synchronous generator regardless of the grid strength.

In contrast to synchronous generators, voltage phase angle jump at the infinite bus can create significant voltage drops at the terminal of GFL-IBRs as illustrated in Figure 8 depending on the SCR of the grid. This behaviour can be explained by the current source nature of GFL-IBRs.

Voltage drops created at the terminal of the GFL-IBRs by voltage phase angle jump in the upstream grid can impact their behaviour during disturbances. This is because the fault ride-through mechanism of GFL-IBRs is voltage-based. It is worth noting that voltage drop induced by voltage phase angle jump at the terminal of the GFL-IBR disappears as the PLL locks to the new voltage phase angle. As such, the performance of the GFL-IBR in response to voltage drop caused by voltage phase angle jump at the upstream grid depends on the dynamics of the PLL in GFL-IBRs. This underlines the importance of EMT studies.

An important observation in Figure 8 is that positive voltage phase angle jump creates voltage rise at the terminal of the GFL-IBR. Voltage rise at the terminal of the GFL-IBRs due to the positive voltage phase angle jump can trigger the overvoltage protection and disconnect the IBR. Voltage rise induced by the positive voltage phase angle jump at the terminal of the GFL-IBR disappears as the PLL locks to the new voltage phase angle. As such, the operation of the instantaneous overvoltage protection of GFL-IBRs depends on the dynamics of the PLL. This again underlines the importance of EMT studies.

Another factor that impacts the relationship between voltage phase angle jump at the infinite bus and voltage drop at the terminal of GFL-IBRs is the operating point of the IBR as illustrated in Figure 9. As illustrated in Figure 9, voltage drop at the terminal of the GFL-IBR increases from 0 to 0.13 pu when the injected active power of the IBR changes from 0 to 1 pu for voltage phase angle jump equal to 30° at the infinite bus.

As illustrated in Figure 10, voltage phase angle jump at the terminal of the synchronous generator is almost independent of voltage phase angle jump at the infinite bus regardless of the grid strength. Again, this is because of the voltage source nature of the synchronous generator. This explains why in classic studies disturbance-induced voltage phase angle jump at the infinite bus was not a major concern.

In contrast to synchronous generators, voltage phase angle jump at the terminal of the GFL-IBRs highly depends on voltage phase angle jump at the infinite bus. It can further be observed in Figure 10 that the SCR of the grid is a crucial factor in determining the relationship between voltage phase angle jump at the infinite bus and voltage phase angle jump at the terminal of the GFL-IBRs.

Another factor that influences the relationship between voltage phase angle jump at the infinite bus and voltage phase angle jump

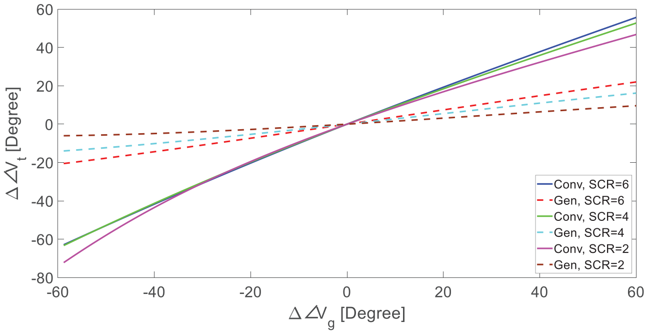

FIGURE 10 | Change in the voltage phase angle jump due to voltage phase angle jump at the infinite bus for different grid strengths. Synchronous generator and GFL-IBR cases are shown by dashed and solid curves, respectively.

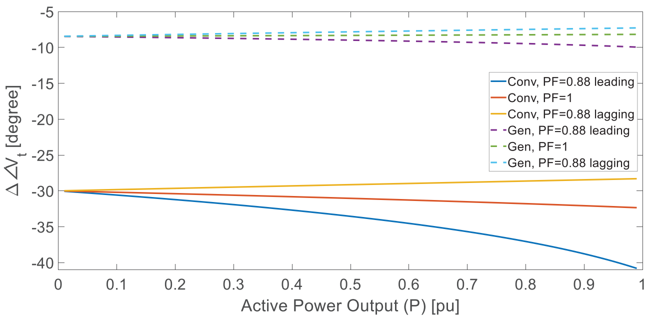

FIGURE 11 | Change in the voltage phase angle jump due to voltage phase angle jump equal to −30° at the infinite bus for different operating points. Synchronous generator and GFL-IBR cases are shown by dashed and solid curves, respectively.

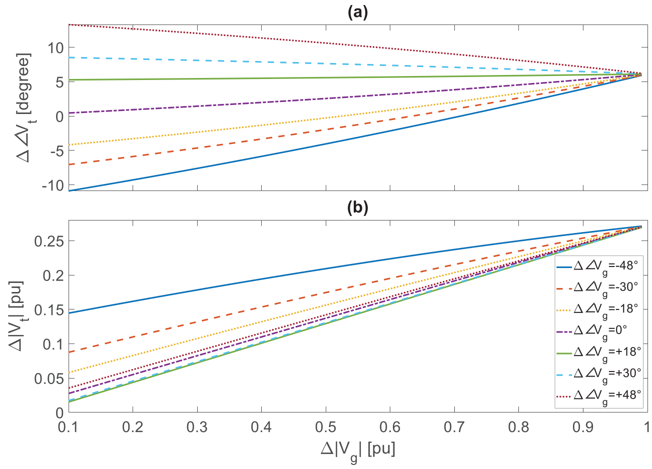

FIGURE 12 | Change in (a) voltage phase angle and (b) voltage magnitude of a synchronous generator due to a combination of voltage drop and voltage phase angle jump at the infinite bus when SCR = 4.

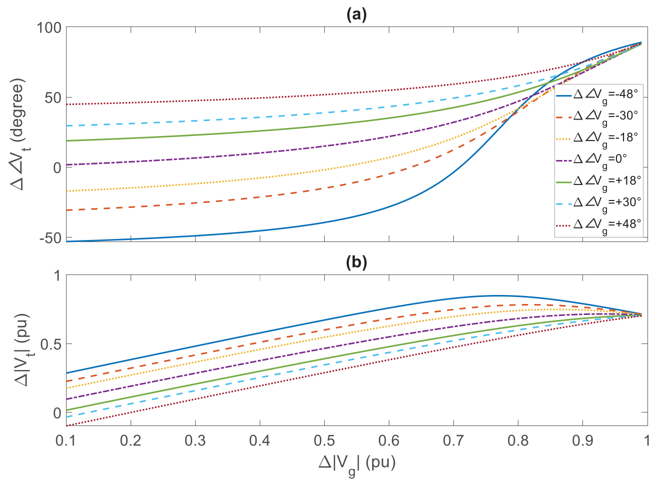

FIGURE 13 | Change in (a) voltage phase angle and (b) voltage magnitude of a GFL-IBR due to a combination of voltage drop and voltage phase angle jump at the infinite bus when SCR = 4.

at the terminal of the GFL-IBRs is the operating point of the IBR as illustrated in Figure 11. As illustrated in Figure 11, voltage phase angle jump at the terminal of the GFL-IBR can increase from 30° to 41° when the injected active power of the GFL-IBR changes from 1 to 0 pu for the voltage phase angle jump equal to 30° at the infinite bus. Figure 11 also underlines the impact of the output power factor of the GFL-IBR. For example, voltage phase angle jump increases from 28° to 41° when power factor changes from 0.88 lagging to 0.88 leading.

2.3.3 | A Combination of Voltage Drop and Voltage Phase Angle Jump at the Infinite Bus

The findings in the previous sections underline the importance of considering both voltage drop and voltage phase angle jump when analysing the behaviour of GFL-IBRs during disturbances. In this section, the impact of a combination of voltage phase angle jump and voltage drop at the infinite bus on voltage characteristic at the terminal of synchronous generators and GFL-IBRs are examined based on the formulations derived in Sections 2.1 and 2.2.

As illustrated in Figure 12, voltage drop and voltage phase angle jump at the terminal of a synchronous generator is not substantially impacted by voltage drop and voltage phase angle jump at the infinite bus. For example, consider a case in which voltage drop and voltage phase angle jump at the infinite bus are 0.5 pu and zero, respectively. Voltage drop and voltage phase angle jump at the terminal of the synchronous generator are equal to 0.14 pu, and 2.5°, respectively. Voltage drop of 0.5 pu with voltage phase angle jump of −30° at the infinite bus creates voltage drop of 0.17 pu and voltage phase angle jump of −2° at the terminal of the synchronous generator. Moreover, voltage drop of 0.5 pu with voltage phase angle jump of 30° at the infinite bus creates voltage drop of 0.13 pu and voltage phase angle jump of 7.5° at the terminal of the synchronous generator. As illustrated in Figure 12, voltage drop changes at the terminal of the synchronous generator caused by voltage phase angle jump at the infinite bus is intangible.

In contrast to synchronous generators, voltage drop and voltage phase angle jump at the terminal of a GFL-IBR is highly dependent on both voltage drop and voltage phase angle jump in the upstream grid as illustrated in Figure 13. Figure 13 clearly

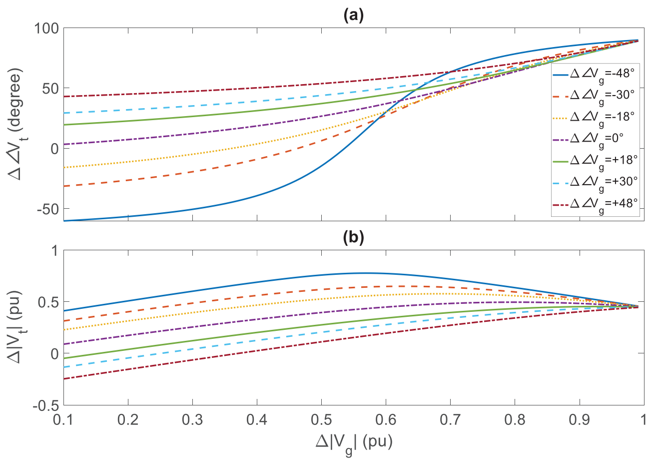

FIGURE 14 | Change in (a) voltage phase angle and (b) voltage magnitude of a GFL-IBR due to a combination of voltage drop and voltage phase angle jump at the infinite bus when SCR = 2.5.

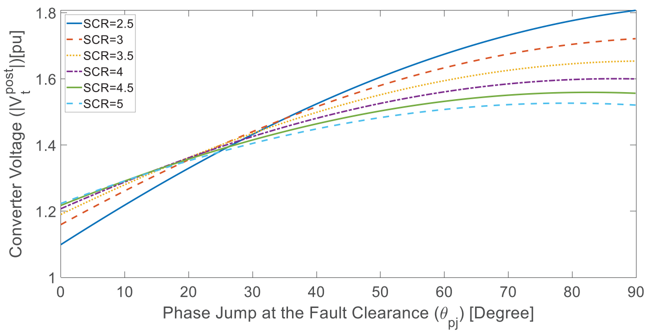

FIGURE 15 | Voltage magnitude at the terminal of the GFL-IBR at the instant of the fault clearance for different grid strengths.

indicates the impact of the combination of voltage drop and voltage phase angle jump at the upstream grid in determining voltage drop and voltage phase angle jump that appears at the terminal of a GFL-IBR.

As illustrated in Figure 13, all the curves converge to the same point for severe voltage drops at the infinite bus. This indicates when the voltage drop at the infinite bus is severe the impact of voltage phase angle jump is intangible. Thus, the impact of voltage phase angle jump can be ignored for GFL-IBRs that are close enough to the location of a severe fault. Nevertheless, the combination of voltage drop and voltage phase angle jump must be considered for understanding the dynamic behaviour of the GFL-IBRs that are far enough from the location of a disturbance not to experience severe voltage drops at their upstream bus. This observation can further explain why a fault hundreds of miles away can trigger voltage phase jump protection of GFL-IBRs as observed in the Odessa events in 2021 and 2022. It is worth noting that the combination of voltage drop and voltage phase angle jump at the upstream grid have higher impact on GFL-IBRs in weaker grids as illustrated in Figure 14.

2.4 | Special Case of Voltage Phase Angle Jump Recovery at the Instant of the Fault Clearance

In this section, we demonstrate the instantaneous overvoltage protection can be triggered by the dynamic response of GFL-IBRs to voltage phase angle jump recovery at the instant of the fault clearance. This was one of the largest contributors to the tripping of the GFL-IBRs in the Odessa disturbance events in 2021 and 2022.

The methodology used here is similar to the methodology employed in Section 2.2. However, we need to consider the fault ride-through mechanism of the GFL-IBR. The current output of the inverter during the fault is regulated by the terminal voltage magnitude of the inverter. In order to avoid overly complicated analysis, the following assumptions are made: (1) The PLL is synchronised to the new phase angle after the fault occurrence; (2) the voltage support mechanism is active; (3) the PLL phase angle and the IBR current remain unchanged right after the fault clearance; and (4) the current controller loop is ideal.

The output current of the IBR can be derived considering the above mentioned assumptions as given in (13)–(14).

$$I_{c,q}^{\text{fault}} = \min\left\{I_{\max},\quad K_{\text{factor}} \times (1 - V_{t,d}^{\text{fault}})\right\} \tag{13}$$

$$I_{c,d}^{\text{fault}} = \min\left\{\sqrt{I_{\max}^2 - (I_{c,q}^{\text{fault}})^2},\quad \frac{P}{V_{t,d}^{\text{fault}}}\right\} \tag{14}$$

where $I_{c,d}^{\text{fault}}$ and $V_{t,d}^{\text{fault}}$ denote the IBR current and voltage during fault in the d axis, respectively. $I_{c,q}^{\text{fault}}$ and $V_{t,q}^{\text{fault}}$ denote the IBR current and voltage during fault in the q-axis, respectively. $V_{t,q}^{\text{fault}}$ is assumed to be zero. $I_{\max}$ denotes the maximum allowable current of the inverter. K_{factor} denotes the voltage support parameter of the inverter. P denotes the pre-disturbance reference active power of the inverter.

The upstream bus voltage during fault and after the fault clearance is given by (15) and (16), respectively. θ_{pj} denotes the voltage phase angle recovery at the instant of the fault clearance. Voltage at the terminal of the GFL-IBR is calculated by (17) at the instant of the fault clearance.

$$|V_g^{\text{fault}}|\angle\theta_g^{\text{fault}} = V_t^{\text{fault}} - X_g I_c^{\text{fault}} \tag{15}$$

$$\overline{V}_g^{\text{post fault}} = 1\angle\left(\theta_g^{\text{fault}} + \theta_{pj}\right) \tag{16}$$

$$\overline{V}_t^{\text{post fault}} = jX_g \overline{I}_c^{\text{fault}} + \overline{V}_g^{\text{post fault}} \tag{17}$$

Figure 15 illustrates the voltage magnitude at the terminal of the GFL-IBR at the instant of the fault clearance. As illustrated in Figure 15, the magnitude of $\overline{V}_t^{\text{post fault}}$ never violates the 1.3 pu threshold when recovery voltage phase angle jump at the upstream grid is 0°. However, the magnitude of $\overline{V}_t^{\text{post fault}}$ exceeds the 1.3 pu threshold when the recovery voltage phase angle jump at the upstream grid is large enough. This can trigger the instantaneous overvoltage protection. Recently, it is recommended by NERC in [8] to both increase the time delay and setting of the instantaneous overvolatge protection. As suggested in [8], further study are needed to confirm the effectiveness of the proposed solution. Figure 15 illustrates that the proposed solution may not be sufficient in some cases.

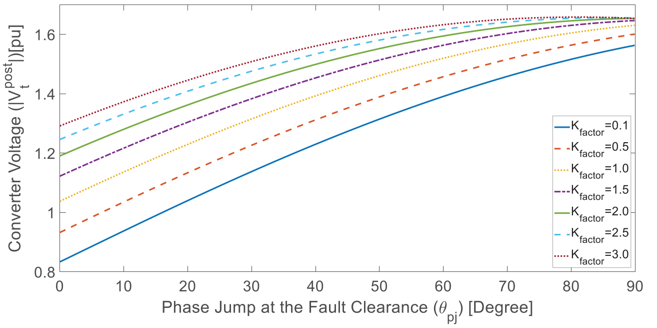

FIGURE 16 | Voltage magnitude at the terminal of the GFL-IBR at the instant of the fault clearance for different K_{factor}.

There are several influencing factors that impacts the voltage magnitude rise at the terminal of the GFL-IBRs due to recovery voltage phase angle jump at the upstream grid such as K_{factor} and the strength of the grid. Figure 16 illustrates the impact of K_{factor} on the $\overline{V}_t^{\text{post fault}}$. As expected, the voltage rise magnitude and the possibility of triggering the overvoltage protection increases at higher K_{factor} values. It is worth noting that the results presented here are produced considering the above mentioned assumptions. Thus, EMT studies are required to obtain more accurate results and check the possibility of harmful overvoltage conditions.

3 | System-Wide Analyses of Disturbance-Induced Voltage Drop and Voltage Phase Angle Jump

In the previous sections, it is demonstrated voltage characteristics at the terminals of GFL-IBRs are determined by voltage drop and voltage phase angle jump at the upstream grid. In this section, we demonstrate voltage drop and voltage phase angle jump at the upstream bus of a GFL-IBR heavily depend on the type and location of the disturbance. As such, we assert that compliance with existing standards is not sufficient to guarantee the proper dynamic performance of GFL-IBRs. Instead, system-wide analyses are required to characterise the characteristics of voltage drop and voltage phase angle jump that might be experienced by the GFL-IBR based on its point of connection to the grid. Afterward, the dynamic performance of GFL-IBRs must be tested and verified based on the characteristics of voltage drop and voltage angle jump obtained through system-wide studies.

The IEEE 39-bus test system, shown in Figure 17, is employed to demonstrate the significance of the system-wide studies for determining the characteristics of voltage drop and voltage phase angle jump at different buses of a grid. The characteristics of voltage drop and voltage phase angle jump at different buses of the IEEE 39-bus test system are illustrated in Figures 18–20 for the cases of mid-line faults, generator tripping and transmission line tripping, respectively. For the sake of conciseness, the results are presented only for bus 16 and bus 29 of the IEEE 39-bus test system. It is assumed that GFL-IBRs will be connected to buses of the IEEE 39-bus test system through transmission lines.

Figure 18 illustrates voltage drops and voltage phase angle jumps experienced at bus 16 and bus 29 of the IEEE 39-bus test system due to the occurrence of mid-line faults at the transmission lines 7, 12, 17, 22, 28, and 42. It is worth noting that these

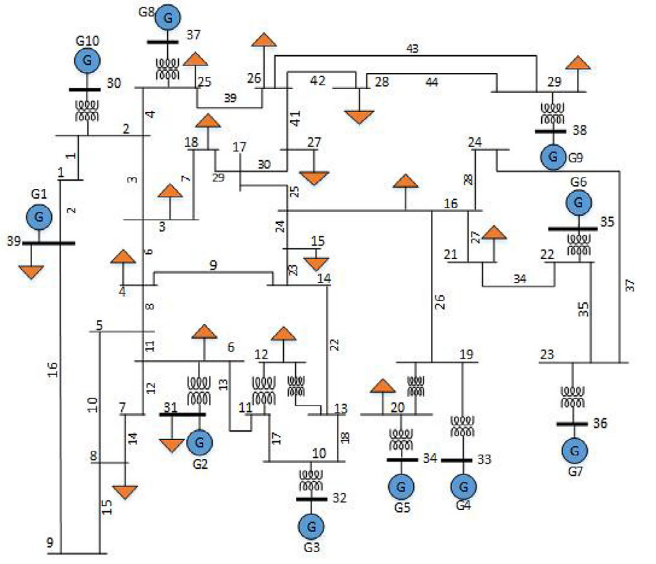

FIGURE 17 | IEEE 39-bus test system.

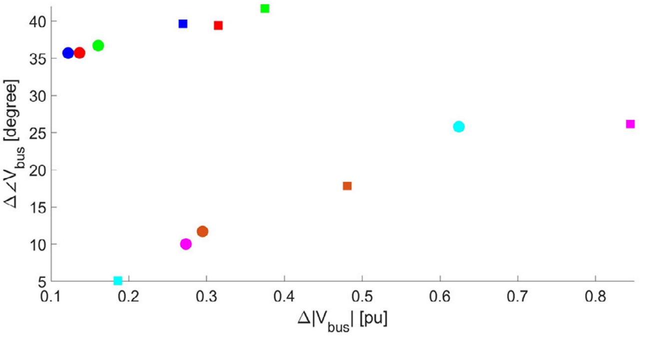

FIGURE 18 | Voltage drop and voltage phase angle jump experienced at bus 16 (illustrated by solid squares) and bus 29 (illustrated by solid circles) for the occurrence of mid-line faults at the transmission lines 7 (brown), 12 (blue), 17 (red), 22 (green), 28 (magenta), 42 (cyan).

voltage drops and voltage phase angle jumps may aggravate at the terminal of the GFL-IBRs depending on the SCR of the connecting transmission line and the operating point of the GFL-IBRs. As illustrated in Figure 18, bus 16 experiences voltage phase angle jump around 40° when voltage drop is between 0.3 and 0.4 pu. This is while bus 29 experiences voltage phase angle jump around 35° when voltage drop is less than 0.2 pu.

Figure 19 illustrates voltage drops and voltage phase angle jumps experienced at bus 16 and bus 29 of the IEEE 39-bus test system due to tripping of generators 2, 4, 6, 8, 9, and 10. Voltage phase angle jumps at bus 16 never exceed −6°. Nevertheless, bus 29 can experience voltage phase angle jump as large as −28°. Voltage phase angle jump of −28° in the upstream bus of a GFL-IBR not only can trigger voltage phase angle jump protection of the inverter but also can activate the fault ride through mechanism of the GFL-IBR despite the small voltage drop at the upstream bus.

Figure 20 illustrates voltage drops and voltage phase angle jumps experienced at bus 16 and bus 29 of the IEEE 39-bus test system due to tripping of transmission lines 3, 11, 12, 17, 26, and 34. As

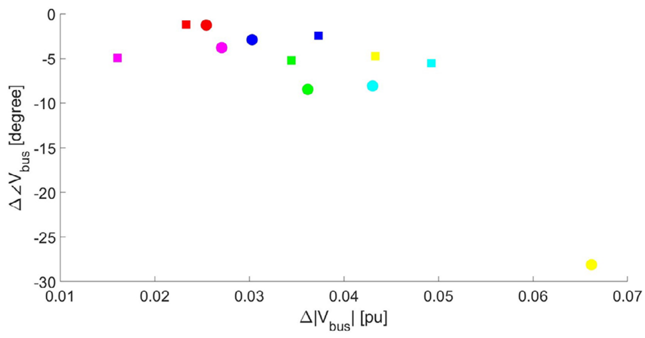

FIGURE 19 | Voltage drop and voltage phase angle jump experienced at bus 16 (illustrated by solid squares) and bus 29 (illustrated by solid circles) for the tripping of generators 2 (blue), 4 (green), 6 (cyan), 8 (magenta), 9 (yellow) and 10 (red).

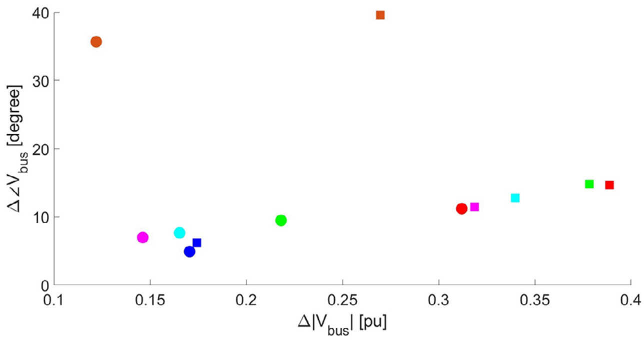

FIGURE 20 | Voltage drop and voltage phase angle jump experienced at bus 16 (illustrated by solid squares) and bus 29 (illustrated by solid circles) for disconnection of transmission lines 3 (brown), 11 (green), 12 (cyan), 17 (magenta), 26 (red) and 34 (blue).

illustrated in Figure 20, bus 16 never experiences voltage drops lower than 0.31 pu. This is while bus 29 experiences voltage drops larger than 0.31 pu for tripping of several transmission lines. This voltage drops can create large voltage drops and voltage phase angle jumps at the terminal of GFL-IBRs connected to bus 29.

Figures 18–20 highlight the differences in voltage characteristics experienced at different buses in a power system. These differences can translate into huge differences in voltage drop and voltage phase angle jump at the terminal of GFL-IBRs depending on the SCR of the connecting transmission line. Moreover, as illustrated in Figures 18–20, faults on transmission lines and transmission line tripping usually create positive voltage phase angle jump while generator tripping create negative voltage phase angle jump. Positive voltage phase angle jump with small voltage drop in the upstream grid can cause instantaneous overvoltage at the terminal of the GFL-IBR and its switches as discussed in Section 2.

4 | Electromagnetic Transient Studies

Phasor-domain analysis is employed in Section 2 to characterise voltage drop and voltage phase angle jump at the terminal of GFL-IBRs at the instant of disturbance occurrence. In this section, EMT simulations are conducted using MATLAB Simulink to test

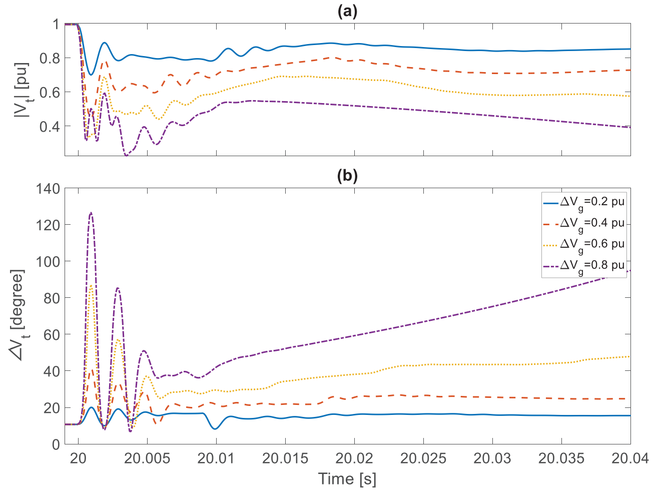

FIGURE 21 | (a) Voltage magnitude and (b) voltage phase angle at the terminal of a GFL-IBR in case of voltage drop without voltage phase angle jump at the upstream bus for grid strength equal to 3.

and verify the previous results. A Type 4 wind generator equipped with low voltage ride through mechanism is used as a GFL-IBR in the simulations. The parameters of the wind generator are provided in the Appendix.

4.1 | Voltage Drop Without Voltage Phase Angle Jump

Figure 21 illustrates the EMT simulations for the single machine infinite bus model when there is voltage drop without voltage phase angle jump at the infinite bus. The SCR of the grid between the infinite bus and GFL-IBR is considered to be equal to 3. As illustrated in Figure 21, voltage drop at the upstream grid can create large voltage phase angle jump at the terminal of the GFL-IBR. This study is focused on disturbances caused by transmission line switching where voltage drop with small phase angel jumps occur.

4.2 | Voltage Phase Angle Jump Without Voltage Drop

Figure 22 illustrates the EMT simulations for the single machine infinite bus model when there is voltage phase angle jump without voltage drop at the infinite bus. The SCR of the grid between the infinite bus and GFL-IBR is again considered to be equal to 3. As illustrated in Figure 22, voltage phase angle jump at the upstream grid not only creates voltage phase angle jump at the terminal of the GFL-IBR but also changes voltage magnitude at the terminal of the GFL-IBR. As previously discussed, positive and negative voltage phase angle jumps at the upstream grid create voltage rise and voltage drop at the terminal of the GFL-IBR, respectively. This study is focused on disturbances caused by generator tripping.

Figure 23 illustrates the impact of the grid strength on the voltage characteristics at the terminal of a GFL-IBR. As illustrated in Figure 23, the grid strength also impacts the dynamics of the PLL in the GFL-IBR. Figure 24 illustrates the impact of the operating

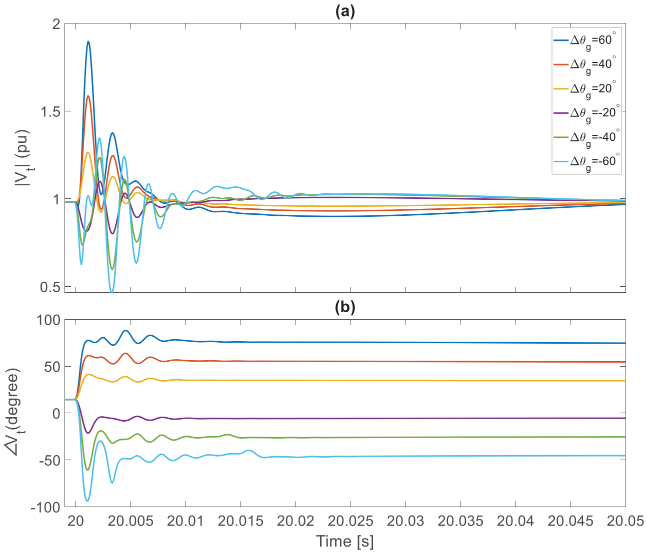

FIGURE 22 | (a) Voltage magnitude and (b) voltage phase angle at the terminal of a GFL-IBR in case of voltage phase angle jump without voltage drop at the upstream bus for grid strength equal to 3.

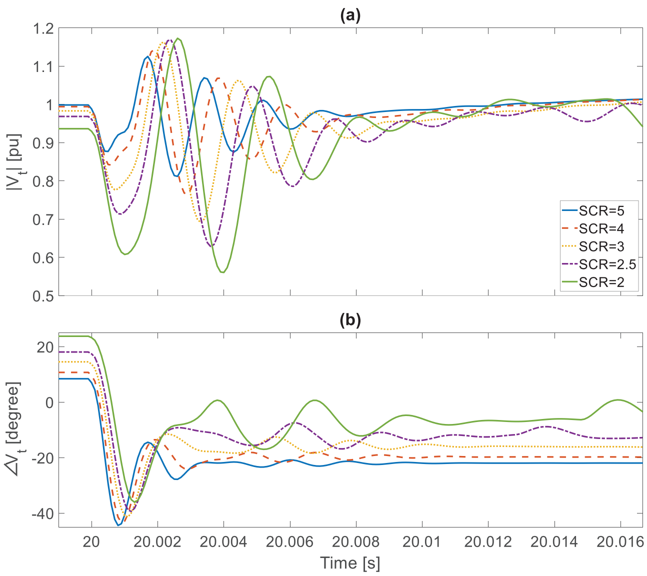

FIGURE 23 | (a) Voltage magnitude and (b) voltage phase angle at the terminal of a GFL-IBR in case of voltage phase angle jump equal to −30° without voltage drop at the upstream bus for different grid strengths.

point on the voltage characteristics at the terminal of a GFL-IBR. As discussed in Section 2.3, the impact of operating point on voltage drop is more considerable compared to voltage phase angle jump.

4.3 | A Combination of Voltage Drop and Voltage Phase Angle Jump

Figure 25 illustrates voltage drops and voltage phase angle jumps at the terminal of a GFL-IBR for various voltage phase angle jumps at the upstream grid when voltage drop at the upstream grid is equal to 0.5 pu. The grid strength is considered to be equal to 4. As shown in Figure 25, voltage drop at the terminal of the

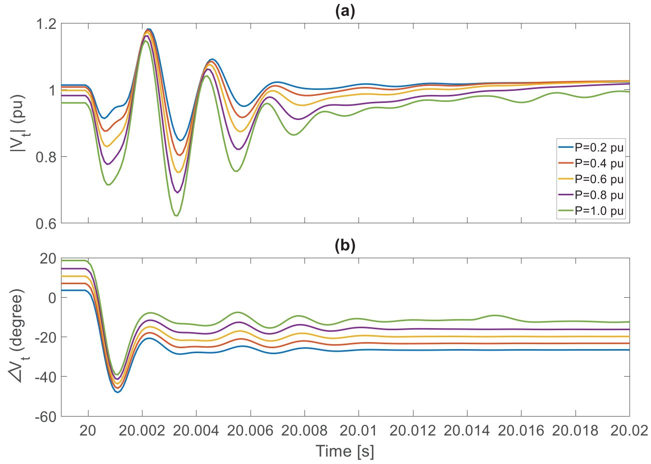

FIGURE 24 | (a) Voltage magnitude and (b) voltage phase angle at the terminal of a GFL-IBR in case of voltage phase angle jump equal to −30° without voltage drop at the upstream bus for different operating points.

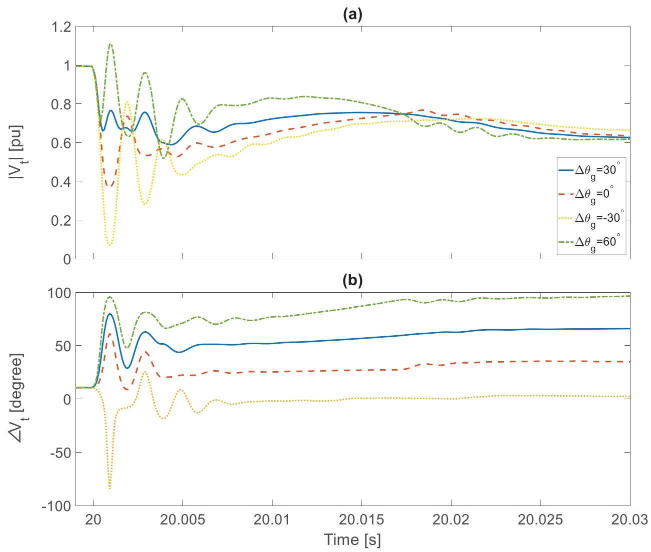

FIGURE 25 | (a) Voltage magnitude and (b) voltage phase angle at the terminal of a GFL-IBR in case of voltage drop equal to 0.5 pu and different voltage phase angle jumps at the upstream bus when SCR = 4.

GFL-IBR significantly depends on the voltage phase angle jump in the upstream grid even when the voltage drop at the upstream grid is fixed. As illustrated in Figure 26, the dynamic response of the GFL-IBR may become completely different depending on the voltage phase angle jump at the upstream grid. It is worth noting that severe voltage drops at the upstream grid mask the impact of voltage phase angle jump at the upstream grid on dynamic response of the GFL-IBR as illustrated in Figure 27. This study is focused on disturbances caused by faults.

Figures 25 and 27 confirm that anti-islanding protection based on voltage phase angle jump is prone to misoperation. As illustrated in these figures, disturbances other than IBR islanding can cause voltage phase angle jumps as large as 60°. A report from National Grid Electric System Operator (ESO) has recently suggested that IBRs should ride-through phase angle jumps as large as 60° [24].

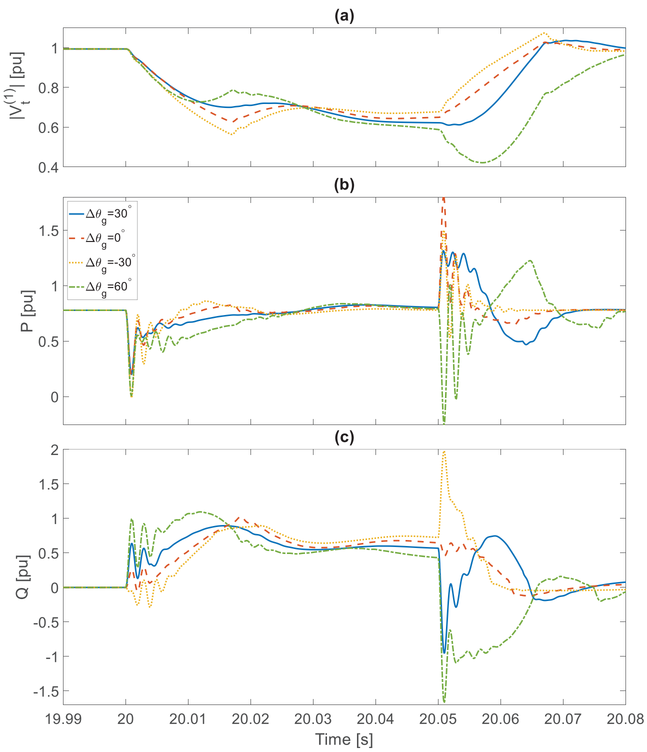

FIGURE 26 | (a) Fundamental component of the terminal voltage and (b) output active power, and (c) output reactive power of a GFL-IBR in case of voltage drop equal to 0.5 pu and different voltage phase angle jumps at the upstream bus when SCR = 4.

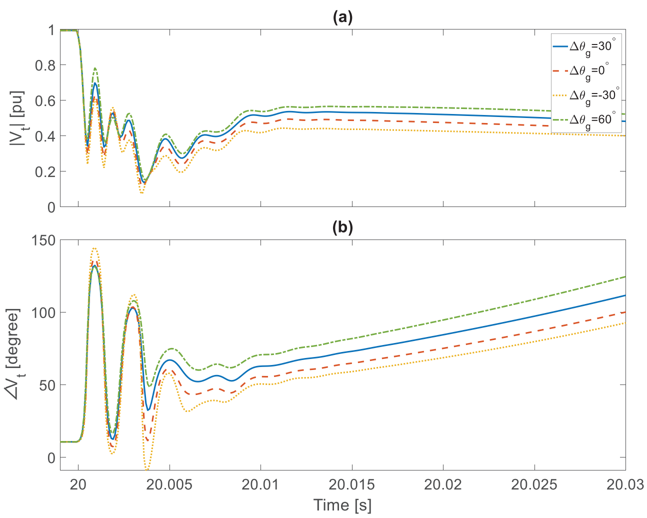

FIGURE 27 | (a) Voltage magnitude and (b) voltage phase angle at the terminal of a GFL-IBR in case of voltage drop equal to 0.8 pu and different voltage phase angle jumps at the upstream bus when SCR = 4.

4.4 | Special Case of Voltage Phase Angle Jump Recovery at the Instant of the Fault Clearance

Figure 28 illustrates the voltage rise at the terminal of the GFL-IBR after the fault clearance. As shown in Figure 28, voltage phase angle jump at the instant of the fault clearance plays a critical role in determining the voltage rise at the terminal of the GFL-IBR. It is worth noting that voltage rise after fault

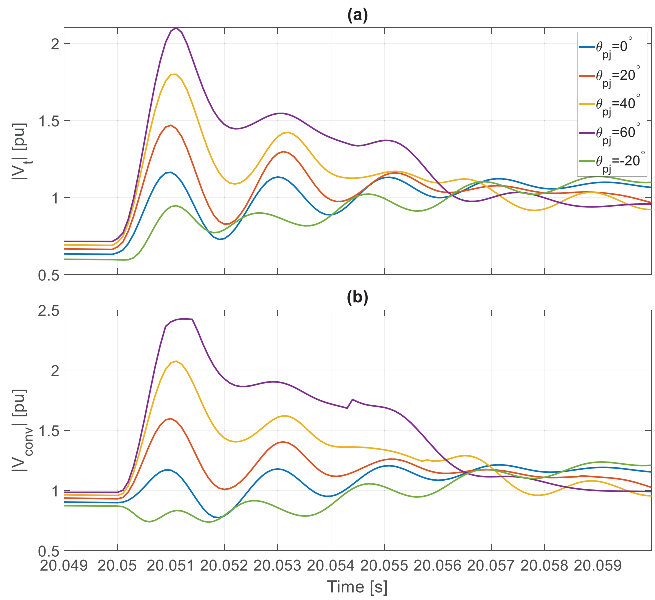

FIGURE 28 | Voltage magnitude at the (a) terminal, (b) converter of a GFL-IBR at the instant of fault clearance for voltage drop equal to 0.5 pu and different voltage phase angle jumps at the upstream bus when SCR = 4.

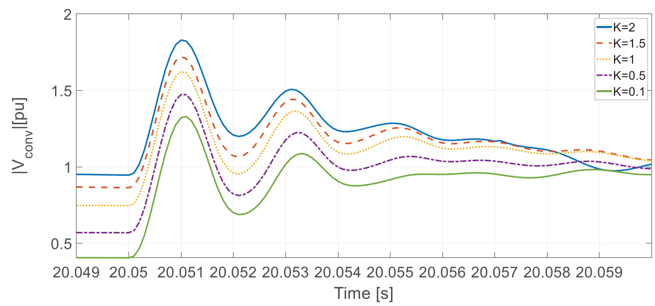

FIGURE 29 | Voltage magnitude at the converter of a GFL-IBR at the instant of fault clearance for voltage drop equal to 0.5 pu at upstream bus and different K_{factor}.

clearance is not concerning when voltage phase angle jump due to fault clearance is equal to zero. Recently, it is recommended by NERC in [8] to both increase the time delay and setting of the instantaneous overvolatge protection to avoid its operation during fault clearance. Figure 28 indicates that the proposed solution may not be sufficient in some cases.

Figure 29 illustrates the impact of K_{factor} on the voltage rise due to fault clearance. As shown in Figure 29, a higher K_{factor} increases the voltage rise due to fault clearance. Figure 30 illustrates the impact of SCR on the voltage rise due to fault clearance. As shown in Figure 30, SCR may impact the voltage rise due to fault clearance differently depending on the voltage phase angle jump at the upstream grid. The voltage rise due to fault clearance is higher at high SCRs when the voltage phase angle jump in the upstream grid is small. Conversely, the voltage rise due to fault clearance is smaller at high SCRs when the voltage phase angle jump in the upstream grid is large. This is discussed in detail in Section 2.4.

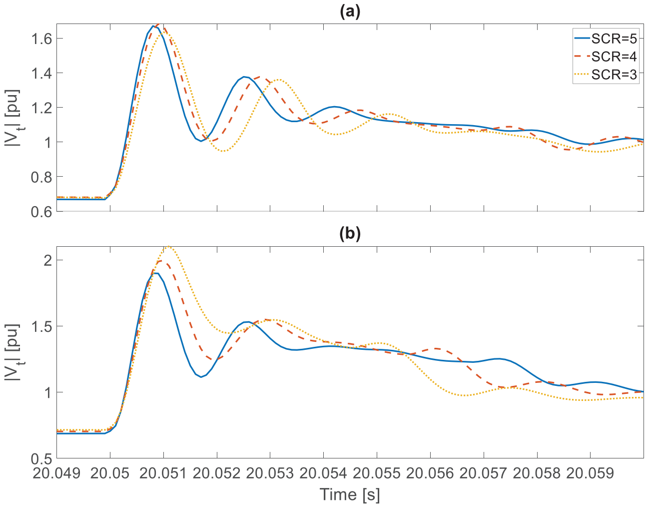

FIGURE 30 | Voltage magnitude at the terminal of a GFL-IBR at the instant of fault clearance for voltage drop equal to 0.5 pu and voltage phase angle jump equal to (a) −30° and (b) −60° for different grid strengths.

5 | Conclusion

This paper investigated the root cause of disturbance-induced misoperation of GFL-IBRs. It is demonstrated that in contrast to synchronous generators, GFL-IBRs can experience severe voltage drop and voltage phase angle jump at their terminals due to voltage drop and voltage phase angle jump in the upstream grid. It is further demonstrated that grid strength and operating point of the GFL-IBRs are critical factors in determining the voltage characteristics at the terminal of GFL-IBRs during disturbances. It is demonstrated that voltage drop and voltage phase angle jump at the terminal of GFL-IBRs depend on the type and location of the disturbance. As such, the dynamic performance of the GFL-IBRs are required to be investigated and verified based on system-wide studies rather than sole compliance with generic response requirements described by standards such as IEEE 1547 and IEEE 2800.

Author Contributions

Negar Karimipour: conceptualization, formal analysis, investigation, methodology, software, validation, visualization, writing – original draft, writing – review and editing. **Mohammadreza F. M. Arani:** conceptualization, formal analysis, funding acquisition, investigation, methodology, project administration, resources, software, supervision, validation, visualization, writing – original draft, writing – review and editing. **Amir Abiri Jahromi:** conceptualization, formal analysis, investigation, methodology, validation, visualization, writing – original draft, writing – review and editing.

Acknowledgements

The authors wish to acknowledge the NSERC Discovery Grants Program.

Conflicts of Interest

The authors declare no conflicts of interest.

Data Availability Statement

Data sharing is not applicable to this article as no datasets were generated or analysed during the current study.

References

1. R. Quint, et al., "Transformation of the Grid: The Impact of Distributed Energy Resources on Bulk Power Systems," *IEEE Power and Energy Magazine* 17, no. 6 (2019): 35–45.

2. A. Sajadi, J. A. Ranola, R. W. Kenyon, B. M. Hodge, and B. Mather, "Dynamics and Stability of Power Systems With High Shares of Grid-Following Inverter-Based Resources: A Tutorial," *IEEE Access* 11 (2023): 29591–29613.

3. "1200 MW Fault Induced Solar Photovoltaic Resource Interruption Disturbance Report," North American Electric Reliability Corporation, published June 8, 2017, https://www.nerc.com/pa/rrm/ea/Documents/1200_MW_Fault_Induced_Solar_Photovoltaic_Resource_Interruption_Final.pdf.

4. "IEEE Standard for Interconnection and Interoperability of Inverter-Based Resources (IBRs) Interconnecting with Associated Transmission Electric Power Systems," in *IEEE Std 2800-2022* (IEEE, 2022), 1–180.

5. "IEEE Standard for Interconnection and Interoperability of Distributed Energy Resources with Associated Electric Power Systems Interfaces," in *IEEE Std 1547-2018 (Revision of IEEE Std 1547-2003)* (IEEE, 2018), 1–138.

6. "Recap of Inverter-Based Resource Panel," in *NERC MRC/BOT Meeting Technical Session*, North American Electric Reliability Corporation, published February 2023, https://www.nerc.com/comm/RSTC/Documents.

7. Joint NERC and Texas RE Staff Report, in *Odessa Disturbance* (North American Electric Reliability Corporation, 2021).

8. Joint NERC and Texas RE Staff Report, in *Odessa Disturbance Texas Event* (North American Electric Reliability Corporation, 2022).

9. A. Hoke, S. Chakraborty, T. Basso, and M. Coddington, "*Beta Test Plan for Advanced Inverters Interconnecting Distributed Resources With Electric Power Systems (NREL/TP–5D00–60931)*," (NREL, 2017).

10. Nelson, et al., *Hawaiian Electric Advanced Inverter Grid Support Function Laboratory Validation and Analysis (NREL/TP–5D00–60931)*, (NREL, 2016).

11. A. Hoke, et al., *Experimental Evaluation of PV Inverter Anti–Islanding With Grid Support Functions in Multi–Inverter Island Scenarios (NREL/TP–5D00–66732)* (NREL, 2016).

12. Nelson, G. Martin, and J. Hurtt, *Advanced Grid Support Functionality Testing for Florida Power and Light (NREL/TP-5D00-67577)* (NREL, 2017).

13. A. Rolan, S. Bogarra, and M. Bakkar, "Integration of Distributed Energy Resources to Unbalanced Grids Under Voltage Sags With Grid Code Compliance," *IEEE Transactions on Smart Grid* 13, no. 1 (January 2022): 355–366.

14. M. Bakkar, S. Bogarra, A. Rolan, F. Corcoles, and J. Saura, "Voltage SAG Influence on Controlled Three-Phase Grid-Connected Inverters According to the Spanish Grid Code," *IET Generation, Transmission and Distribution* 14, no. 10 (February 2020): 1882–1892.

15. D. Celik and M. E. Meral, "Voltage Support Control Strategy of Grid-Connected Inverter System Under Unbalanced Grid Faults to Meet Fault Ride Through Requirements," *IET Generation, Transmission and Distribution* 14, no. 16 (July 2020): 3198–3210.

16. A. A. Aboelnaga, M. A. Azzouz, H. F. Sindi, and A. S. A. Awad, "Fault Ride Through of Inverter-Interfaced Renewable Energy Sources for Enhanced Resiliency and Grid Code Compliance," *IEEE Transactions on Sustainable Energy* 13, no. 4 (October 2022): 2275–2290.

17. R. T. Elliott, A. Ellis, P. Pourbeik, J. J. Sanchez-Gasca, J. Senthil, and J. Weber, "Generic Photovoltaic System Models for WECC—A Status Report," in *Proceedings IEEE Power and Energy Society General Meeting* (IEEE, 2015), 1–5.

18. G. Lammert, L. D. P. Ospina, P. Pourbeik, D. Fetzer, and M. Braun, "Implementation and Validation of WECC Generic Photovoltaic System Models in DIgSILENT PowerFactory," in *Proceedings IEEE Power and Energy Society General Meeting* (IEEE, 2016), 1–5.

19. A. Lorenzo-Bonache, A. Honrubia-Escribano, F. Jimenez-Buendia, and E. Gomez-Lazaro, "Field Validation of Generic Type 4 Wind Turbine Models Based on IEC and WECC Guidelines," *IEEE Transactions on Energy Conversion* 34, no. 2 (June 2019): 933–941.

20. L. Callegaro, G. Konstantinou, C. A. Rojas, N. F. Avila, and J. E. Fletcher, "Testing Evidence and Analysis of Rooftop PV Inverters Response to Grid Disturbances," *IEEE Journal of Photovoltaics* 10, no. 6, (November 2020): 1882–1891.

21. A. Ahmad, H. D. Tafti, G. Konstantinou, B. Hredzak, and J. E. Fletcher, "Distributed Photovoltaic Inverters' Response to Voltage Phase-Angle Jump," *IEEE Journal of Photovoltaics* 12, no. 1 (January 2022): 429–436.

22. L. Fan, Z. Wang, and Z. Miao, "Large Angle Deviation in Grid-Following IBRs Upon Grid Voltage Dip," *IEEE Transactions on Energy Conversion* 39, no. 1 (2024): 368–378.

23. F. Blaabjerg, *Control of Power Electronic Converters and Systems: Vol. 3*, 1st ed. (Elsevier Science and Technology, 2021).

24. "Great Britain Grid Forming Best Practice Guide," National Grid ESO, published April 2023, https://www.nationalgrideso.com/document/278491/download.

Appendix

2 MVA PMSG, $K_{\text{factor}} = 2$, $PI_{\text{pll}} = 35.5+631.6/s$, $PI_P = 0.001+314.2/s$, $PI_Q = 0.1+50/s$, $PI_I = 0.962+36.3/s$, $L_f = 0.2$ pu, $R_f = 0.02$ pu, $C_f = 0.05$ pu.